Mechatronics 65 (2020) 102294

Contents lists available at ScienceDirect

Mechatronics

journal homepage: www.elsevier.com/locate/mechatronics

Technical note

Energy harvesting using piezoelectric transducers for suspension systems☆

Rafael Tavares*, Michael Ruderman

Faculty of Engineering and Science, University of Agder (UiA), Grimstad, Norway

ARTICLE INFO

Keywords:
Energy harvesting
Piezoelectric transducer
Two-port model
System identification
Electromechanical system

ABSTRACT

Energy harvesting by using functional materials in suspension systems bear potential to win-back certain (even if low) amounts of vibrational energy, otherwise dissipated via the conventional (passive) dampers. Piezoelectric (PE) ceramics are functional materials that can be used for transforming mechanical energy into electrical and vice versa. In this paper, we study the capabilities and efficiency of energy harvesting (EH) with PE transducers under two different kinds of external excitation: i) Periodic and ii) stochastic. An appropriate nonlinear lumped parameter electromechanical model (LPEM) is brought into the two-port network notation. Laboratory experiments were conducted under periodic external force-controlled excitation performed on a universal test machine (UTM). The two-port model parameters were identified and the model was validated by comparing results of numerical simulations and experiments. Extended simulations have been conducted to investigate the EH capabilities of PE transducers in automotive applications, i.e. EH in suspension systems under the standardized road conditions. The analysis results of the power conversion and EH efficiency are presented and discussed.

1. Introduction

Piezoelectric (PE) materials have been intensively used in actuation systems which require precision in micro- and nano-positioning, such as micromanipulators, micro-valves, atomic force microscopes, adaptive optics, ultra-precision machine tools, but also structural dampers, see e.g. [7,11] and references therein for overview. PE materials are favorable due to being compact, lightweight and with high precision and bandwidth response [7]. Despite being mostly known for their use as actuators, the exhibited piezoelectric effect can be divided into two – direct and converse. When an electric field is applied between the electrodes, it produces a mechanical strain which can be used for actuation and positioning control (converse effect). On the contrary, a PE material induces an electric potential when stressed (direct effect), that can be used for sensing applications, such as in electro-acoustic transducers, pressure sensors in touch pads or tilt sensors, widespread in consumer electronics [29].

Over the last decades, PE materials have been actively investigated also in energy harvesting (EH) applications, mainly due to their high actuation frequency range, relatively high power density and bidirectional coupling between the mechanical and electrical properties. For more extensive overview on the use of PE materials in energy harvesting applications we refer to the several sources [2,4,20,24,31,33].

If properly integrated into inherently-vibrating structures, the PE materials, with their high stiffness, can be seen as auxiliary harvesting, yet not necessarily actuating, elements. At that point, one should distinguish between harvesting and, otherwise common in nowadays technologies, recuperation mode. Semi-active and active suspension systems, in general, constitute a potential application field for a PE-based harvesting operation. Chassis technology for high-end cars are already successfully evolving towards the active or semi-active electro-(magneto-)mechanical suspensions. An associated more flexible and targeted tuning of the vibration damping shows significant improvement in ride performance, both in terms of handling (tire deflection) and comfort (sprung mass acceleration, suspension deflection, harshness) simultaneously [25]. Harvesting the energy, otherwise dissipated by the shock absorbers, is potentially advantageous, since a reduction of the overall power consumption is required for improving the fuel economy, bringing down emissions, and supplying the power demand of additional subsystems [40] in a vehicle. Most of the research literature on simultaneous damping and energy harvesting address a complex approach that can require a re-design of the suspension system as a whole [1,41]. High power-weight ratio and high (mechanical-to-electrical energy) conversion efficiency solutions have been and remain of high relevance in industrial applications. Those alternatives that can be added into existing shock absorber solutions, without major constructive modifications, are

☆ This research receives funding from the European Community Horizon 2020 Research and Innovation Programme (H2020-MSCA-RISE-2016) under the Marie Skłodowska-Curie grant agreement no. 734832.

* Corresponding author.
E-mail addresses: rafael.tavares@uia.no (R. Tavares), michael.ruderman@uia.no (M. Ruderman).

https://doi.org/10.1016/j.mechatronics.2019.102294
Received 18 May 2019; Received in revised form 20 September 2019; Accepted 27 October 2019

of the most importance. The present paper aims to contribute toward further investigations with a feasibility study on the EH potential of PE transducers in the suspension systems.

1.1. Piezoelectric modeling approaches

The most conventional description of the piezoelectricity was published by the standards committee of the IEEE [12] as linearized constitutive equations

$$S_p = s_{pq}^{E} T_q + d_{kp} E_k \tag{1}$$

$$D_i = d_{iq} T_q + \varepsilon_{ik}^{T} E_k \tag{2}$$

The constitutive equations state that the material strain S_p and electrical displacement D_i are linearly related to the mechanical stress T_q and the electrical field E_k. The piezoelectric constant d, permittivity ε, and elastic compliance s are the material constants, while the i, k, p and q subscripts indexes indicate the directions of displacement and polarization (see [8,12] for more in detail explanation). The superscripts E and T denote that those constants are evaluated at constant electric field and constant stress, respectively. Despite describing uniformly the general relationship between the electrical and mechanical domain, equations (1), (2) lack to capture both nonlinearities and dynamic transients, typical for PE actuators and transducers. To those belong a rate-independent hysteresis [5], creep and vibrations [17]. Furthermore, the linear constitutive coefficients can turn out as temperature-dependent and show an additional (strong) electric field dependency.

Various modeling approaches have been proposed in the literature for the electromechanical behavior of PE materials, see for example [11] and references within for a survey. In order to account for both forward and feedback interactive couplings between the electrical and mechanical domains (and correspondingly both direct and converse PE effects), a rather physics or domain-oriented modeling approach is required, as referred e.g. in [7,29].

For applications envisaging the EH and potential damping adjustment of a PE transducer, a physically reasoned electromechanical interpretation that can be compatible with two-port network modeling [26] and incorporation of two-way coupling effects is needed. A most notable approach was introduced with the lumped parameter electromechanical model (LPEM) proposed in [8,9], that managed to postulate the principal behavioral phenomena evidenced by PE transducers. More details on LPEM model and its inclusion into the two-port network formulation are given later in Section II. An extension of LPEM was also proposed in [27], where the state-varying capacitance and Voigt-Kelvin-type linear creep effects were augmented to the standard LPEM form and experimentally evaluated on a commercial PE-stack actuator.

1.2. Contribution and outline of work

This paper provides experimental and numerical simulation studies on EH when using a PE transducer, under the periodic and stochastic excitations. The LPEM model is explicitly brought into a generalized two-port notation. This re-structure of the model with introduction of new port variables (force, velocity, voltage and current) is suitable for describing the bidirectional PE effects and further convenient for energy-based analysis. The hysteretic behavior observed in the electric domain is included with the nonlinear extension, modeled by play-type operators with identified parameters from experimental data. A series of laboratory experiments under force-controlled external excitation are conducted on an universal test machine (UTM), and also used for identification of the free model parameters, and subsequent model evaluation. In particular, for mechanical excitation cycles we measure and analyze the harvested energy output of the PE transducer under stress. The obtained experimental results, for various frequencies, amplitudes, excitation forces and resistive loads are used to conclude on the EH efficiency under periodic excitation. Note that some preliminary results of experimental investigation have been also reported recently in [35]. After validating the assumed model, our goal is to investigate the EH efficiency when using the PE transducer in vibration-based applications where the external excitation is rather of a stochastic nature. Numeric simulations were conducted for a desired case, i.e. the EH in automotive suspension systems under the standardized road profile conditions.

The structure of the main part of the paper is as follows. In Section 2, the nonlinear electromechanical lumped parameter model of PE is brought into the two-port network notation. Section 3 introduces different notations and definitions of EH efficiency, while we specify those assumed in the recent study according to the nature of input excitation. The experimental evaluation of the PE transducer performed under periodic conditions is described in Section 4, along with description of the experimental setup, parameter identification, model validation and evaluation of the EH efficiency. A simulation study of the experimentally validated PE model incorporated in a vibration-based energy harvesting application, which is conventional quarter-car passive suspension system, is described in detail in Section 5. Finally, conclusions and brief outlook are presented in Section 6.

2. PE model

2.1. Electromechanical lumped parameter model (LPEM)

The assumed modeling approach is based on the lumped parameter electromechanical model originally introduced in [8,9]. The LPEM describes the behavior of a 1-DOF (degree of freedom) PE-element brought into a topology consisting of the electrical and mechanical subsystems, leading to the ordinary differential equations describing the principal dynamic system behavior. Considering mechanical domain of a PE transducer as a mass-spring-damper system with mass m, open-lead stiffness[1] k and damping coefficient b, the mechanical dynamics is governed by

$$m\ddot{x} + b\dot{x} + kx = F_t + F, \tag{3}$$

where F_t is the transduced force, representing coupling with electrical domain, and F is the external mechanical force applied to PE transducer.

In the electric domain, the PE transducer is mainly governed by a capacitive behavior, since PE materials are dielectric. Experimental observations [8,9] disclosed hysteresis between the voltage and displacement, as well as between the force and displacement under the shorted electrode leads. However, since there is no hysteresis observed with the open electrode leads, but it is observed between displacement and charge when they are closed, the LPEM model rationally concluded the hysteresis lying in the electrical domain of PE transducers. Note that this basic assumption is also inline with PE fundamentals, see e.g. [5].

Following to LPEM one assumes that the net electrical charge q_p, across the PE, is given by the sum of two components

$$q_p = q_c + q_t, \tag{4}$$

where the voltage across the capacitor is defined by

$$q_c = C v_t, \tag{5}$$

with C to be the electrical capacitance of PE at constant strain. Recall that the electrical and mechanical domains are coupled via the direct and converse PE effects, so that charge q_t is induced due to the relative displacement x (which is the PE stroke). The transduced force F_t is proportional to the capacitor voltage, so that the electromechanical couplings between both domains are given by

$$q_t = T x, \tag{6}$$

$$F_t = T v_t. \tag{7}$$

[1] The open-lead stiffness k is the stiffness of the piezoelectric transducer measured in open-circuit, without the influence of nonlinear terms.

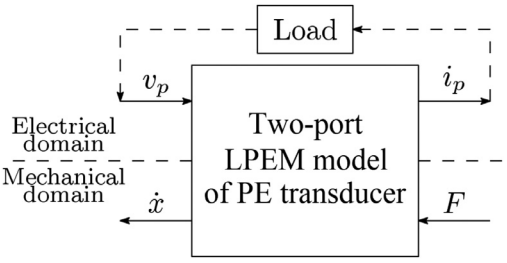

Fig. 1. Two-port network model for the PE transducer.

Here the constant transformer ratio is denoted by T.

The nonlinearity, introduced by hysteresis, between the overall charge and voltage [8] can be expressed as

$$v_h = H(q_p), \tag{8}$$

while the total terminal voltage, i.e. between the PE electrodes, is given by

$$v_p = v_t + v_h. \tag{9}$$

It is worth noting that the PE charge is generally challenging to measure, in practice. That means the resulting current $i_p = \dot{q}_p$ flowing through the PE transducer can be rather measured when the PE leads are in a closed circuit.

2.2. Two-port network formulation

Generic models of a two-port network transducer can be applicable for most types of reciprocal power-converting elements, in particular for electrostatic, piezoelectric, electromagnetic and electrodynamic, see e.g. [14,26]. A standard two-port model of an transducer can be defined by its across and through variables. The across variable for an electrical element is voltage and the through variable is current. The across variable for mechanical element is force, while the through variable is the displacement rate, i.e. relative velocity. The two-port formulation is convenient for energy analysis, since the power can be directly obtained by multiplying the corresponding across and through variables.

The transfer characteristics of a PE element are governed by mechanical and electrical subdynamics. A simple linear two-port PE transducer can be, therefore, directly formulated from linear the constitutive Eqs. (1) and (2), as has been done in [26] for estimating the maximum output power and efficiency of the system. Yet, one should keep in mind that a PE transducer two-port model is a bidirectionally coupled 2×2 multi-input-multi-output (MIMO) system which is nonlinear, in general terms. Therefore, our goal is to use a two-port model formulation suitable of describing both actuating and sensing transducers' effects. Obviously, the model formulation relies on the above mentioned principles of a two-port network model for PE, and the LPEM equations given in (3)-(9). The resulting two-port network model of PE transducer with port variables F, $\dot{x}$, v_p and i_p is depicted by block-diagram in Fig. 1.

2.3. Hysteresis modeling

The hysteresis between the voltage and charge is described in [8,27] using the so-called Maxwell-slip structure, which coincides with the Prandtl-Ishlinskii (P-I) stop-type hysteresis model, see e.g. [28] for details. According to the implemented two-port PE model, the hysteresis can be inversely captured by

$$q_p = H^{-1}(v_h), \tag{10}$$

and therefore implemented by using the P-I play-type operators. Hysteretic play-type operators are well-known in mechanics and often used to describe a kinematic play, also known as backlash. It provides a multi-valued rate-independent map under a common input v for each operator.

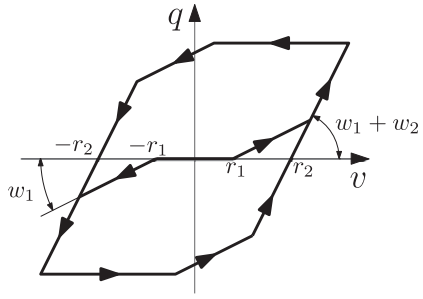

Fig. 2. Schematic representation of P-I play-type hysteresis model with superposition of two operators [35].

The play-type operator dynamics can be described also in a differential form [28] as

$$\dot{q} = \begin{cases} w\dot{v} & \text{if} \quad \frac{q}{w} - r = v \ \text{ or } \ \frac{q}{w} + r = v, \\ 0 & \text{if} \quad \frac{q}{w} - r < v < \frac{q}{w} + r. \end{cases} \tag{11}$$

Recall that the P-I type models can be used for describing both forward and inverse hysteresis, and allow for a fast analytical computation. With superposition of multiple play-type operators, as exemplary illustrated in Fig. 2, it is possible to sufficiently map a real hysteresis behavior while assuming a relatively small number of the free parameters. Note that the classical P-I model can characterize only symmetric and rate-independent hysteresis behavior. Each operator is defined by two parameters, the dead-band width r_j and the slope w_j, with $j = \{1, 2, 3\}$. Increasing the number of operators leads to increasing smoothness of the input-output hysteresis map and, as implication, to higher (local) accuracy of the P-I model. At the same time it largely increases the complexity of properly determining the distributed model parameters.

3. Efficiency of energy harvesting

Vibration suppression and energy harvesting by a PE transducer can be done by shunting the free leads to an impedance [23]. Recall that due to bidirectional couplings, the PE transducer can convert energy from the mechanical to the electrical domain and vice versa. The energy conversion in PE transducer reveals how much of the power supplied by vibrations gets actually converted into electricity. The subsequent removal of converted electrical energy from a PE transducer necessarily results in additional structural damping [18].

When referring to energy harvesting, the term efficiency is generally associated with energy conversion efficiency, i.e. the ratio of output to input energy in a harvesting system. Although, there is no consistency between multiple authors when it comes to definition of the efficiency term, being often presented as ratio of energy as in [21,38] or also in terms of a power ratio as in [10,26,32].

In numerous studies the efficiency is commonly expressed analytically, as a relation to the electromechanical coupling factor squared [10,26], which represents how efficient is the PE material alone, in terms of the energy conversion. Although, this definition does not account for structural design and further contributing aspects the connected electrical circuit. Therefore, the total EH efficiency is mostly significantly smaller than the material coupling factor [38].

Several analytical expressions have been deducted, as shown in the literature, in order to calculate the theoretical maximum value of efficiency. An upper limit of 46% has been reported in [32], considering the efficiency of energy conversion by assuming a load resistance which can actively change to the maximize power output. Such upper limit has been argued by [16], stating that the efficiency could reach 80%, while no experimental evidence can be found for that. It is obvious that large discrepancies in efficiency values are directly linked to the viewpoint taken for the definition and additional assumptions about energy

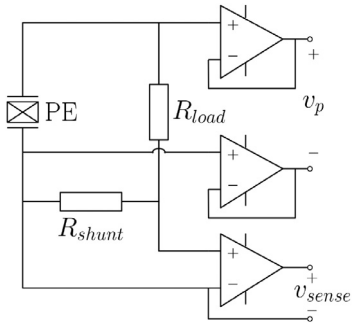

Fig. 3. Electronic circuit for voltage and current measurement.

losses. Ratios of energy per cycle are of a large interest when describing the applications associated with a periodic excitation, for instance cantilever vibration harvesters [21,26]. At the same time, when facing excitations of a stochastic nature, a definition of efficiency in terms of average power appears as more appropriate.

In this work, we define the efficiency of energy harvesting η depending on the principal signals' pattern of the applied excitation. For periodic excitations, we consider the efficiency as given by

$$\eta_{\mathrm{P}} = \frac{\tilde{E}_{out}}{\tilde{E}_{in}} = \frac{\tilde{E}_{ele}}{\tilde{E}_{mec}}, \tag{12}$$

with $\tilde{E}$ to be the average energy per cycle. On the contrary for non-periodic excitations, the efficiency we assume is given by

$$\eta_{\mathrm{NP}} = \frac{\tilde{P}_{out}}{\tilde{P}_{in}} = \frac{\tilde{P}_{ele}}{\tilde{P}_{mec}}, \tag{13}$$

where $\tilde{P}$ is the average power in terms of a spectral distribution. For the available experimental setup conditions, only periodic excitations were experimentally evaluated (see Section 4), while non-periodic excitations were further evaluated in simulations (see Section 5). In a PE-based harvesting system, P_{in} is the mechanical power input supplied by a force excitation, and P_{out} is the electrical power output, both given by

$$P_{mec} = F\dot{x} \quad \text{and} \quad P_{ele} = v_p i_p \tag{14}$$

respectively.

The maximum power $\hat{P}$, of a uniform periodic excitation where each cycle is defined between t_1 and t_2, is given by

$$\hat{P} = \max(P(t)),\ t \in [t_1, t_2]. \tag{15}$$

Finally, the energy per cycle $\tilde{E}$ can be obtained by numerical integration of (14), while the energy losses dissipated in a PE transducer (due to damping and coupling effects) can be expressed by

$$E_{loss} = E_{mec} - E_{ele}. \tag{16}$$

4. Experimental study

4.1. Experimental setup

The experimental setup, used in this work, consists of a PE transducer under compressive load excitation, as described in [35] in more details. During experiments, four variables are being monitored, the excitation force F applied to PE element, the relative displacement correspondingly stroke of the prestressed PE element x, the voltage v_p across the two electrodes of PE element, and the current i_p flowing through the overall closed circuit. In the experimental study, only periodic signal excitations were considered due to equipmental restrictions of the laboratory setup.

The measuring circuit includes a resistive load and a shunt resistance ($R_{shunt} = 100\ \Omega$) for current measurement, as shown in Fig. 3. A current sense amplifier was used to increase the voltage output of the current shunt resistance (TI INA213), resulting in the measured voltage v_{sense}

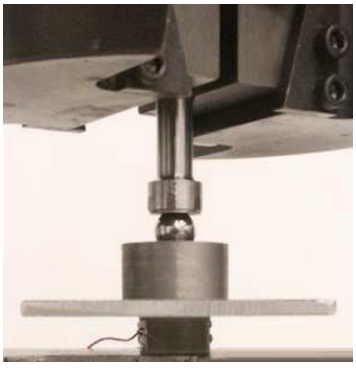

Fig. 4. Laboratory view of the PE in the UTM.

with an amplification factor of 50. Two other operational amplifiers (AD8510) were used as buffers for measuring the voltage between the electrode ends of the PE stack. Three different impedances were used as a passive load: $R_{load} = \{51.43, 97.78, 143.8\}$ kΩ.

The specimen was tested using an UTM from SI-Plan. Due to characteristics of the servohydraulic actuator of the UTM, only periodic excitations were experimentally realized. Several load experiments were conducted under compression using two types of the force loads: step and sinusoidal. The experiments carried out under step load excitations consisting in a periodic repetition of a step force applied during 5 seconds, followed by the release of the force. Experiments were carried out with different loads $F_{step} = \{0.50, 0.75, 1.00, 1.25\}$ kN. The experiments with sinusoidal load profile were conducted under different maximum peak forces $F_{\max} = \{0.50, 0.75, 1.00, 1.25, 1.50\}$ kN, and for different frequencies $f = \{1, 2, 3, 4, 5\}$ Hz. Note that the sinusoidal excitation frequencies f are relatively low comparing to the high resonance frequencies of the PE transducer. A minimum peak force offset around 0.1 kN was applied to avoid loss of a mechanical contact due to no compression forces.

The force measurements were provided by the load cell installed in the servo-hydraulic actuator of the UTM. The used load cell SI-Plan S8390 is with ± 25 kN range, sensitivity 0.593 mV/V, and 700 Ω bridge. For determining offset voltage for zero load, to be subtracted from the analog voltage output, the corresponding calibration curves have been used. The stroke x of the PE is measured by a laser-optical displacement sensor (Micro-Epsilon ILD2300-2, measuring range: 2 mm, resolution: 0.03 μm) configured in a direct reflection mode. The sensor provides a configurable analog voltage output through the C-Box conditioning signal unit. A 3D-printed frame was fabricated to allow the adjustment of the measurement range and the fixture of the sensor to the bottom frame of the machine. The laboratory view of the developed PE setup under load excitation in the UTM is shown in Fig. 4. To guarantee a uniform load distribution over the PE surface and minimize the effects of minor misalignments between the top clamp and bottom frame of the machine, the load was applied into a sphere joint and then transferred to the PE through a steel rod. An additional metal plate was added to create a reflection surface for the laser beam. The analog signals monitored during experiments were collected using a dSpace MicroLabBox via the standard BNC connectors. The analog measuring input channels have a voltage range of ± 10 V followed by an ADC with a resolution of 16 bit, while the sampling rate was set to 1 kHz.

4.2. Experimental results

The measured relative displacement (respectively stroke) x, current i_p and voltage v_p, recorded during two exemplary taken force load experiments, are depicted in Fig. 5 and Fig. 6 ($R_{load} = 51.43$ kΩ). The voltage and current peaks, cf. Fig. 5, resulting from the step force loading, reflect the charge flowing through the PE as a result of change of PE polarization due to mechanical stress. On the contrary, the output current

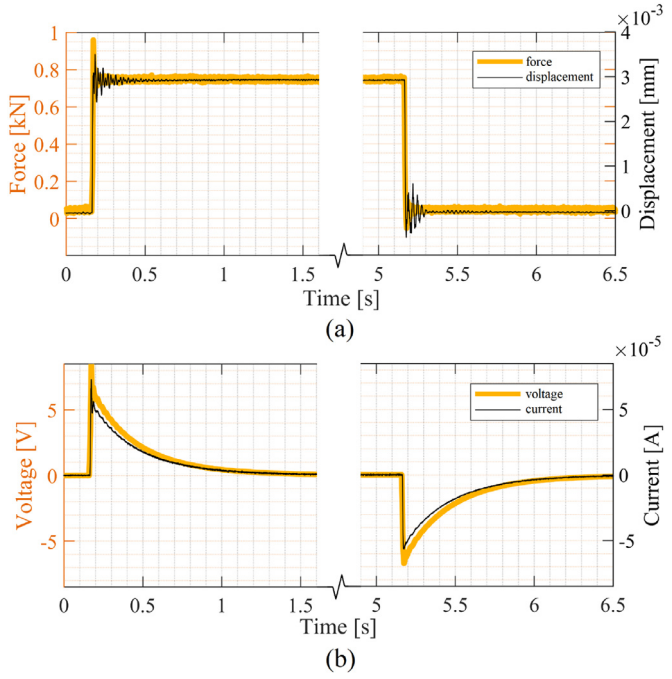

Fig. 5. Measured PE response under step load excitation: (a) force and displacement; (b) voltage and current (R_{load} = 51.43 kΩ).

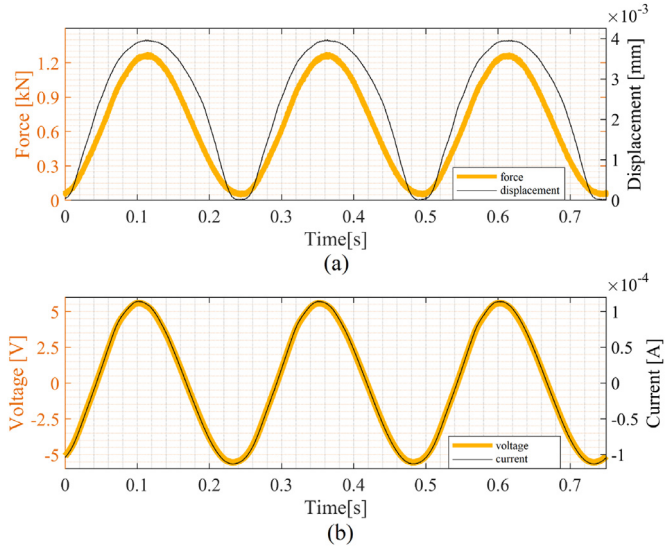

Fig. 6. Measured PE response under sinusoidal load excitation: (a) force and displacement; (b) voltage and current (R_{load} = 51.43 kΩ).

and voltage are also symmetrical sinusoidal signals under a sinusoidal load, cf. Fig. 6. The hysteresis between the voltage and displacement, as well as between the force and displacement were equally observed, cf. with [8,9]. From the sinusoidal load excitation under different frequencies, one sees that for low frequencies (1–5 Hz) the overall measured hysteresis remains truly rate-independent, as shown in Fig. 7. Here one should notice that an expectable stretching, correspondingly rounding, of the hysteresis curves at higher frequencies, are largely related to the coupled subdynamics (with the corresponding phase lag) of the overall electromechanical system. Those spurious interpretations of the measured input-output PE characteristics, involving relative displacement, are sometimes reported as rate-dependent PE hysteresis, while an isolated PE hysteresis in electrical domain is rate-independent, cf. [5,8]

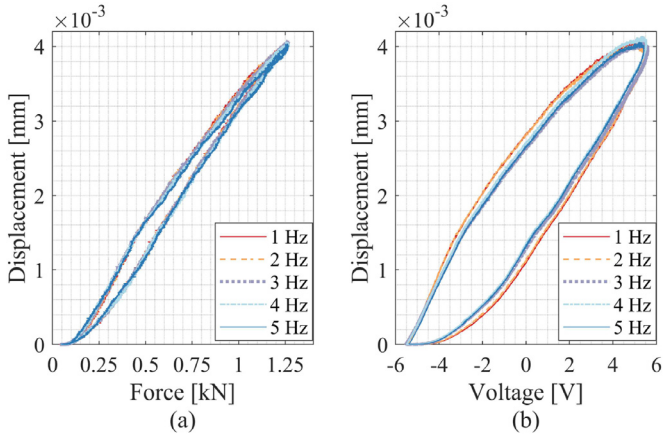

Fig. 7. Measured hysteresis: (a) displacement-force; (b) displacement-voltage (R_{load} = 51.43 kΩ).

Table 1
$\tilde{E}_{ele}$ and $\hat{P}_{ele}$ for step excitation.

Force (kN)	R_{load} (kΩ)	$\tilde{E}_{ele}$ (mJ)	$\hat{P}_{ele}$ (mW)
0.50	51.43	0.594	0.579
0.50	97.78	0.519	0.339
0.50	143.8	0.470	0.257
0.75	51.43	1.397	1.484
0.75	97.78	1.213	0.856
0.75	143.8	1.090	0.634
1.00	51.43	2.450	2.386
1.00	97.78	2.123	1.366
1.00	143.8	1.908	0.996

Table 2
$\tilde{E}_{mec}$ and $\hat{P}_{mec}$ for step excitation.

Force (kN)	R_{load} (kΩ)	$\tilde{E}_{mec}$ (mJ)	$\hat{P}_{mec}$ (mW)
0.50	51.43	15.241	24.623
0.50	97.78	15.163	24.655
0.50	143.8	15.540	25.111
0.75	51.43	31.997	46.927
0.75	97.78	28.925	47.124
0.75	143.8	29.246	48.172
1.00	51.43	45.359	73.847
1.00	97.78	44.665	77.284
1.00	143.8	44.807	76.928

Based on (14), one can estimate the average electrical energy which can be harvested per cycle (one cycle also considers the step load and step unload) and the corresponding power peaks. Newton–Cotes Simpson's rule was used for the discrete numerical integration of the power quantities. The velocity $\dot{x}$ was obtained via numerical differentiation of the measured stroke. A Butterworth third order low-pass filter with cut-off frequency of 100 Hz was applied afterward to the determined $\dot{x}$, in order to remove the effects of derivative signal noise. The same filter was applied to the measured force F so as to introduce the same phase lag and, therefore, allowing for unshifted calculation of the P_{mec}, and correspondingly E_{mec}, values.

The values obtained under different experimental conditions are grouped and summarized in Tables 1 and 2 for the step excitation, and in Tables 3 and 4 for the sinusoidal excitation.

4.3. Identification of model parameters

The two-port model was parameterized for a commercially available PE ring stack transducer (Noliac NAC2125-H10). The overall mass was calculated from the geometry and density of the material. The mechanical stiffness k was calculated using the blocking force and free endpoint

Table 3
$\tilde{E}_{ele}$ and $\hat{P}_{ele}$ for sinusoidal excitation ($R_{load} = 51.43$ kΩ) .

f (Hz)	F = 0.5 kN $\tilde{E}_{ele}$ (mJ)	F = 0.5 kN $\hat{P}_{ele}$ (mW)	F = 0.75 kN $\tilde{E}_{ele}$ (mJ)	F = 0.75 kN $\hat{P}_{ele}$ (mW)	F = 1 kN $\tilde{E}_{ele}$ (mJ)	F = 1 kN $\hat{P}_{ele}$ (mW)
1	0.22	0.04	0.57	0.12	1.02	0.21
2	0.34	0.08	0.94	0.21	1.70	0.36
3	0.39	0.08	1.20	0.25	1.93	0.39
4	0.41	0.09	1.26	0.26	2.02	0.41
5	0.42	0.09	1.28	0.26	2.08	0.42

Table 4
$\tilde{E}_{mec}$ and $\hat{P}_{mec}$ for sinusoidal excitation ($R_{load} = 51.43$ kΩ).

f (Hz)	F = 0.5 kN $\tilde{E}_{mec}$ (mJ)	F = 0.5 kN $\hat{P}_{mec}$ (mW)	F = 0.75 kN $\tilde{E}_{mec}$ (mJ)	F = 0.75 kN $\hat{P}_{mec}$ (mW)	F = 1 kN $\tilde{E}_{mec}$ (mJ)	F = 1 kN $\hat{P}_{mec}$ (mW)
1	11.01	2.57	20.80	4.20	31.14	6.78
2	21.11	4.33	41.34	8.29	61.94	12.52
3	32.04	6.39	65.24	12.60	92.34	18.84
4	42.91	8.32	88.67	18.95	123.14	26.17
5	53.81	11.01	112.59	24.68	155.62	34.43

Table 5
Determined system parameters.

Variable	Description	Value	Units
m	Mass	0.0158	kg
b	Damping coefficient	885.6	Ns/m
k	Open-lead stiffness coefficient	2.596×10^8	N/m
R_{load}	Load impedance	51.43	kΩ
C	Capacitance	3.2	μF
T	Electromechanical coupling	10.698	–
r_1	P-I operator 1 threshold	0.094	μF
r_2	P-I operator 2 threshold	0.213	μF
r_3	P-I operator 3 threshold	0.584	μF
w_1	P-I operator 1 slope	1.2	V/μF
w_2	P-I operator 2 slope	0.8	V/μF
w_3	P-I operator 3 slope	2.3	V/μF

displacement to the rated voltage, nominal values provided by the supplier. The nominal value of linear electrical capacitance C is also available from the datasheet of the PE transducer. The initial values (prior to identification) for the unknown damping coefficient b and electromechanical coupling ratio T were assumed from the previously published research studies, cf. [8].

The residual model parameters, see in (3)–(9), were identified from the experimental measurements. The P-I hysteresis model was discretized with $n = 3$ elements.[2] The r_j and w_j parameters have been identified simultaneously with the damping coefficient b and transformer ratio T. The parameters identification used the minimization of

$$\min \int \left[W_i \big(i(t) - \hat{i}(t)\big)^2 + W_x (x(t) - \hat{x}(t))^2 \right] dt, \tag{17}$$

where $\hat{i}(t)$ and $\hat{x}(t)$ are two-port model estimated outputs for current and displacement, and $W_i = 1/\text{mean}(|i|)$ and $W_x = 1/\text{mean}(|x|)$ are the weighting coefficients. The measured data collected under the excitation conditions $F_{\max} = 0.50$ to 1.25 kN were used for parameter identification, while 1.5 kN was used for evaluation of the identified model under sinusoidal loads. The determined system parameters are listed in Table 5. The comparison between the experimental response of the PE transducer and its two-port model-based prediction are visualized in Figs. 8 and 9, for the step and sinusoidal loads correspondingly. The transient and steady-state match of both predicted output quantities (electrical and mechanical) with the real system response verify the validity of the identified two-port model and argue in favor of its use for further studies.

[2] Simulations shown that 3 elements were sufficient to shape the hysteresis, and further increasing the number of elements does not further improve the accuracy in the model response.

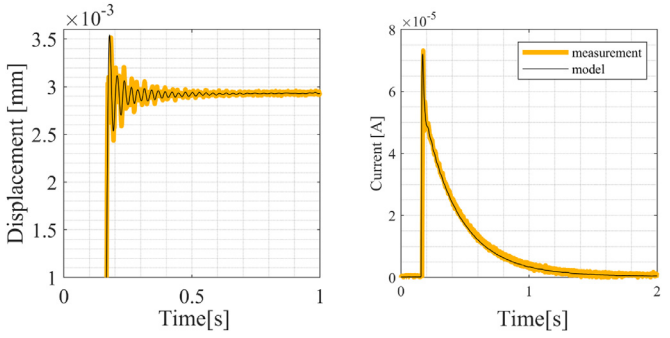

Fig. 8. Measured and model predicted displacement and current response to a step load ($F_{step} = 1.25$ kN).

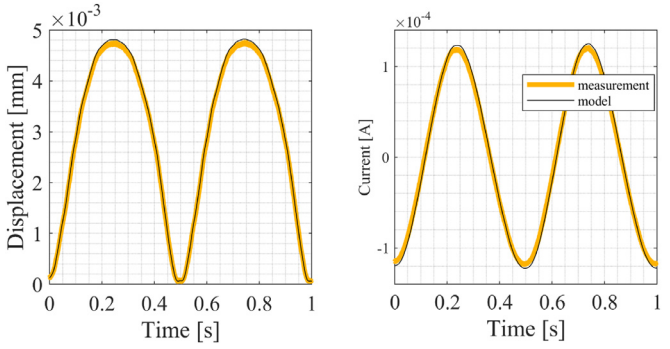

Fig. 9. Measured and model predicted displacement and current response to a sinusoidal load ($F_{\max} = 1.5$ kN and $f = 2$ Hz).

4.4. Efficiency of energy harvesting

In the sinusoidal force solicitation, it is notable that the harvesting potential saturates as the frequency increases, due to the resistive circuit load. The harvesting potential can be further increased by using the synchronized switch harvesting inductor (SSHI) techniques [19,37], which consist in adding up a switching circuit in parallel with the PE element. In SSHI harvesting methods, the PE voltage is always increasing, except during the switch which inverts the PE voltage at each peak, and has always the same sign as the velocity $\dot{x}$. However, an explicit design and implementation of the optimized harvesting load circuits for the PE transducer are out of scope of the recent study and, therefore, subject to the future works.

Fig. 10 visualizes the variation in the obtained average electrical and mechanical energies, $\tilde{E}_{ele}$ and $\tilde{E}_{mec}$, over $F_{\max}$ and f under the sinusoidal load. Note that the power dissipated by the load resistance is minor when compared with the power provided by the mechanical load excitation. At the same time, the PE shunt-damping introduced by the resistance R_{load} reduces the mechanical vibration and, consequently, the total harvested energy. The harvesting power can be increased by tuning the shunt-circuit impedance to the excitation frequency.

The efficiency of EH under periodic excitation is calculated by (12) for periodic excitations. The variation of efficiency η_{P}, with the different F_{step} and R_{load}, is shown in Fig. 11 for the step excitations. The variation of efficiency η_{P}, with the different F_{max} and frequencies f, is shown in Fig. 12 for the sinusoidal excitations. The maximal EH efficiency of 4.9% was obtained for the sinusoidal excitation under the described laboratory conditions. In the literature, an estimated theoretical efficiency is reported to be significantly higher, see e.g. [38]. The obtained experimental results are in line with other experimental stud-

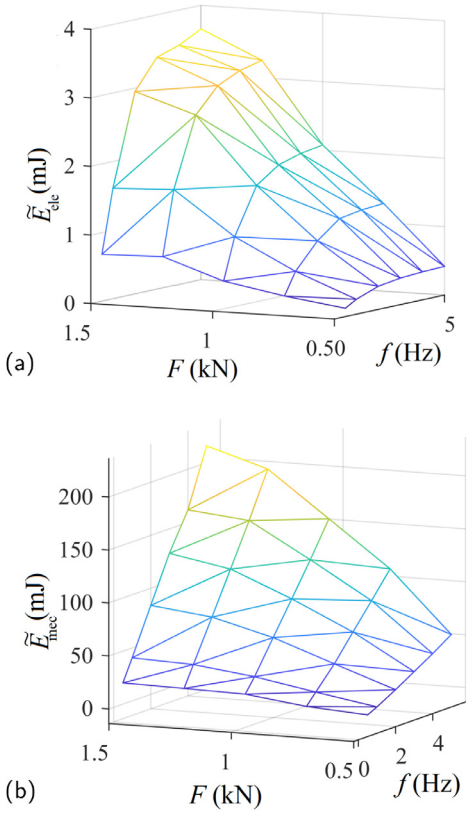

Fig. 10. Variation of $\tilde{E}_{ele}$ in (a) and $\tilde{E}_{mec}$ in (b), for different F_{max} and f of the sinusoidal excitation.

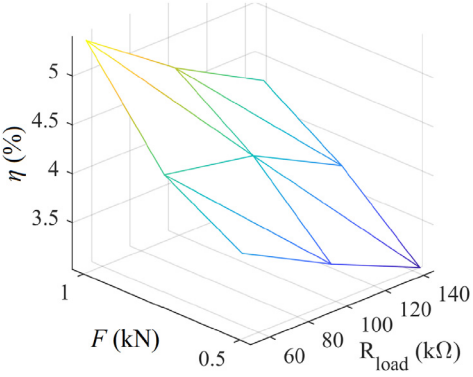

Fig. 11. Efficiency η_P for step excitation.

ies reporting results of much lower efficiency ranging from 1 to 10%. For PZT (lead zirconate titanate), studies report efficiencies of 7.5% for mechanical vibrations in the range of 50–150 Hz with amplitude of 1 kN [15], 5.4% for sinusoidal cantilever vibration in the range of 20–60 Hz [39], 3.1% for < 100 Hz excitation of a PE laminate sandwiched between two Terfenol-D discs [3], 1.2% for impact-based harvesters in low frequency vibrations (< 30 Hz) [13] and 10% for a fixed-fixed beam with ball mass drop impact [36].

5. Simulation study with suspension system

5.1. System description

In order to analyze more realistic aperiodic EH cases, consider a practical application of EH in an automotive suspension. We assume a single corner of a ground vehicle, i.e. the standard quarter-car model with in-

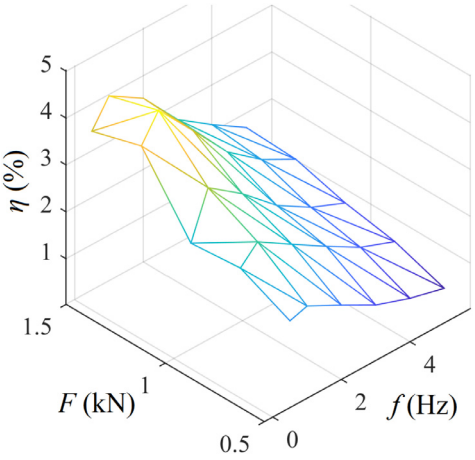

Fig. 12. Efficiency η_P for sinusoidal excitation.

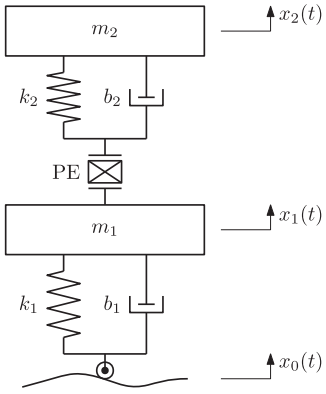

Fig. 13. Diagram of the quarter-car suspension model augmented by the PE transducer.

teractions between the suspension system, the tire, and the chassis as a two degrees-of-freedom system. This allows to study the vibrational response of the vehicle to a road-induced excitation. The PE transducer is introduced between the suspension rod and the unsprung mass, as shown in Fig. 13. This setup allows for analyzing the EH behavior of an structure-integrated PE transducer, while the road excitation x_0 is defined according to the ISO standard 8608.

Applying the Newton's second law, the dynamic equations of suspension system can be written as

$$m_1\ddot{x}_1 = k_1(x_0 - x_1) + b_1(\dot{x}_0 - \dot{x}_1) - F, \tag{18}$$

$$m_2\ddot{x}_2 = k_2(x + x_1 - x_2) + b_2(\dot{x} + \dot{x}_1 - \dot{x}_2), \tag{19}$$

while assuming 1/4 of the vehicle chassis mass m_2, the unsprung mass m_1, the tire stiffness coefficient k_1, the tire damping coefficient b_1, the spring stiffness coefficient k_2, the damping coefficient b_2, the unsprung mass (wheel) displacement x_1, the suspended mass (chassis) displacement x_2, and the kinematic road excitation x_0. The terms x, $\dot{x}$ and F represent the relative displacement, velocity, and applied force variables, respectively, as they used before in the PE two-port model.

5.2. Standardized road profiles

The standard ISO 8608 defines classification of the longitudinal road profiles based on the vertical displacement power spectral density (PSD). For an extensive comparison of the parameters used to simulate the road profiles based on the ISO 8608 we refer to [22], for overview and references therein. The road roughness is typically represented as a stationary stochastic Gaussian process, with the displacement power spectral

Table 6
Road roughness S_0 [m^2/(cycle/m)] at reference spatial frequency ν_0 according to ISO 8608 classification.

Road class	S_0 range, $\times 10^{-6}$	S_0 mean, $\times 10^{-6}$
A (Very good)	< 8	4
B (Good)	8 – 32	16
C (Average)	32 – 128	64
D (Poor)	128 – 512	256
E (Very poor)	512 – 2048	1024

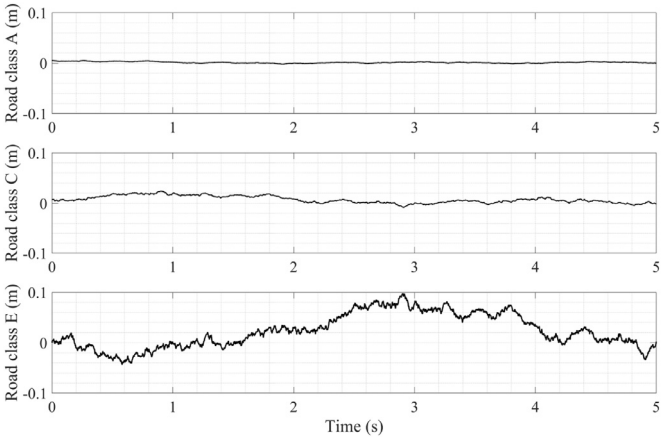

Fig. 14. Sections of the generated input profiles for the road classes A, B and C.

density (PSD) in m^2/(cycle/m) units, given by

$$S_{\mathrm{PSD}}(\nu) = G_r \nu^{\beta}. \tag{20}$$

Here ν is the spatial frequency (cycle/m), $G_r = S_0/\nu_0^{\beta}$ is the road roughness coefficient, S_0 is the displacement PSD at $\nu_0 = 1/(2\pi)$, and a commonly approximated fitting parameter, see e.g. [41], is $\beta = -2$. The ISO classification is based on the value of S_0 as shown in Table 6 (adapted from [41]).

Accurate road excitation PSDs, based on the ISO 8608, can be modeled as white noise input feed through a first-order filter [34,41]. Considering the angular frequency $\omega = 2\pi v \nu$, the PSD of the road excitation can be expressed as

$$S_{\mathrm{PSD}}(\omega) = \frac{2\pi G_r v}{\omega^2 + \omega_0^2}, \tag{21}$$

where v is the longitudinal velocity of the vehicle, and ω_0 is the low-pass filter (LPF) cutoff frequency. Considering the Laplace operator $s = \sigma + j\omega$ for steady-state signal analysis ($\sigma = 0$), the road disturbance, correspondingly excitation, can be then modeled as a white noise signal, filtered by a first-order filter defined as

$$G(s) = \frac{\sqrt{2\pi G_r v}}{s + \omega_0}. \tag{22}$$

G is a linear transfer function of the Laplace variable s. Examples of the road profiles generated through the described method for $v = 50$ km/h are shown in Fig. 14. For instance, the depicted sections of the generated profiles correspond to a drive distance of ≈ 69.4 m.

5.3. Simulation results

The modeled system was simulated with the quarter-car setup, see e.g. [30] for detail. The assumed numerical values, listed in Table 7, are partially based on the used literature [30] and partially on the values available from the automotive suspension manufacturers. For the PE two-port model, the simulation parameters used are previously listed in Table 5. Fig. 15 shows the displacements of the unsprung x_1 an sprung x_2 masses when the vehicle is moving with $v = 50$ km/h on a generated ISO 8608 class C road with input x_0.

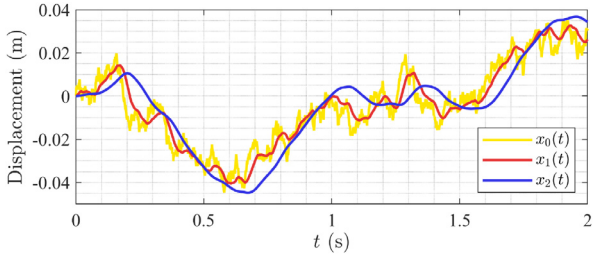

Fig. 15. Simulation of quarter-car on a generated ISO 8608 class C road.

Table 7
Quarter-car simulation parameters.

Variable	Description	Value	Units
m_1	Unsprung mass	50	kg
m_2	Sprung mass	450	kg
k_1	Tire elastic coefficient	200000	N/m
k_2	Passive spring coefficient	50000	N/m
b_1	Tire damping coefficient	1400	Ns/m
b_2	Passive damping coefficient	5000	Ns/m

Table 8
Simulations results of the quarter-car with PE model.

Road class	$\tilde{P}_{ele}$ (mW)	$\tilde{P}_{mec}$ (mW)	η_{NP} (%)
A	0.0271	1.765	1.536
B	0.1108	6.718	1.650
C	0.4774	27.360	1.745
D	1.7541	98.905	1.774
E	7.4179	421.605	1.759

5.4. Efficiency of energy harvesting

The average power $\tilde{P}$ and efficiency η_{NP} are computed by (14) and (13), respectively. The results of the simulation for different class roads are summarized in Table 8.

Other experimental studies in applications with random vibration excitations report an efficiency of 7% with a random vibration signal from 0 to 500 Hz [33], and between 1 and 2% for a bistable system [6]. Despite the low efficiency obtained in simulations, this feasibility study already indicates that the amount of harvested power estimated through simulations seems enough to power some small electronic circuit and sensors placed on the unsprung mass (wheel) of the vehicle.

6. Conclusions

In this paper, we conducted a feasibility study of using PE transducers for energy harvesting, while envisaging applications in suspensions systems. A two-port network model of a PE transducer has been formulated and implemented and the model parameters were identified from experimental data. The two-port model is based on the lumped parameter electromechanical model [8] which couples the electrical and mechanical domains in both directions. Distinct efficiency definitions were introduced for both periodic and stochastic excitations.

Experimental measurements allowed to observe the expected hysteric behavior and transient oscillations. The two-port network model was validated by an accurate prediction of both (electrical and mechanical) output variables in comparison with experimental data under periodic excitations. A maximum EH efficiency $\eta_{\mathrm{P}} = 4.9\%$ was experimentally demonstrated, in line with what have been reported by other studies ranging from 1 to 10%.

The analysis of power in the electrical domain demonstrates the potential capabilities of PE transducers to harvest sufficient energy for supplying small electronic circuits, even though the applied resistive load is not optimal in the recent study. SSHI energy harvesting strategies should be further investigated to improve the EH efficiency.

An accurate prediction of both mechanical and electrical output variables by the derived two-port network model argues in favor of its further use in analysis and design of a PE-based energy harvesting system. To investigate the EH capabilities of PE transducers in suspension systems, we conducted numerical simulations for a classical parameterized quarter-car suspension under generated standard road excitations. For a poor road (ISO 8608 class D), an average power $\tilde{P}_{ele}$ of 1.747 mW can be harvested, according to the numerical simulations which involved the validated two-port PE model. That corresponds to an efficiency of $\eta_{\mathrm{NP}} = 1.77\%$. Experimental evaluations with stochastic load profiles and on real vibration suspension systems are subject of our future works.

Declaration of Competing Interest

The authors declare that they do not have any financial or nonfinancial conflict of interests.

References

[1] Abdelkareem M, Xu L, Ahmed Ali M, Elagouz A, Mi J, Guo S, et al. Vibration energy harvesting in automotive suspension system: a detailed review. Appl Energy 2018;Volume 229:672–99.
[2] Anton SR, Sodano HA. A review of power harvesting using piezoelectric materials (2003–2006). Smart Mater Struct 2007;Volume 16(3):R1.
[3] Bayrashev A, Robbins WP, Ziaie B. Low frequency wireless powering of microsystems using piezoelectric–magnetostrictive laminate composites. Sens Actuators, A 2004;Volume 114(2–3):244–9.
[4] Caliò R, Rongala UB, Camboni D, Milazzo M, Stefanini C, De Petris G, et al. Piezoelectric energy harvesting solutions. Sensors 2014;, Volume 14(3):4755–90.
[5] Damjanovic D. Hysteresis in piezoelectric and ferroelectric materials. Sci Hyster 2006;Volume 3:337–465.
[6] De Paula AS, Inman DJ, Savi MA. Energy harvesting in a nonlinear piezomagnetoelastic beam subjected to random excitation. Mech Syst Signal Process 2015;54:405–16.
[7] Fleming AJ, Leang KK. Design, modeling and control of nanopositioning systems. Springer; 2014.
[8] Goldfarb M, Celanovic N. A lumped parameter electromechanical model for describing the nonlinear behavior of piezoelectric actuators. ASME J Dyn Syst Meas Control 1997;Volume 119(3):478–85.
[9] Goldfarb M, Celanovic N. Modeling piezoelectric stack actuators for control of micromanipulation. IEEE Control Syst Mag 1997;Volume 17(3):69–79.
[10] Goldfarb M, Jones LD. On the efficiency of electric power generation with piezoelectric ceramic. ASME J Dyn Syst Meas Control 1999;Volume 121(3):566–71.
[11] Gu G-Y, Zhu L-M, Su C-Y, Ding H, Fatikow S. Modeling and control of piezo-actuated nanopositioning stages: a survey. IEEE Trans Autom Sci Eng 2016;Volume 13:313–32.
[12] IEEE. IEEE Standard on piezoelectricity. ANSI/IEEE Std 176–1987 1988.
[13] Janphuang P, Lockhart R, Henein S, Briand D, De Rooij N. On the experimental determination of the efficiency of piezoelectric impact-type energy harvesters using a rotational flywheel. In: J Phys: Conf Ser, Volume 476. IOP Publishing; 2013. p. 12137.
[14] Janschek K. The generic mechatronic transducer model – a unified system modeling approach. IFAC Proc Vol 2010;Volume 43(18):267–76.
[15] Kim HW, Batra A, Priya S, Uchino K, Markley D, Newnham RE, et al. Energy harvesting using a piezoelectric cymbal transducer in dynamic environment. Jpn J Appl Phys 2004;Volume 43(9R):6178.
[16] Kim M, Dugundji J, Wardle BL. Efficiency of piezoelectric mechanical vibration energy harvesting. Smart Mater Struct 2015;Volume 24(5):55006.
[17] Leang KK, Zou Q, Devasia S. Feedforward control of piezoactuators in atomic force microscope systems. IEEE Control Syst Mag 2009;Volume 29(1):70–82.
[18] Lesieutre GA, Ottman GK, Hofmann HF. Damping as a result of piezoelectric energy harvesting. J Sound Vib 2004;Volume 269(3–5):991–1001.
[19] Li H, Tian C, Deng ZD. Energy harvesting from low frequency applications using piezoelectric materials. Appl Phys Rev 2014;Volume 1(4):41301.
[20] Liu Y, Tian G, Wang Y, Lin J, Zhang Q, Hofmann HF. Active piezoelectric energy harvesting: general principle and experimental demonstration. J Intell Mater Syst Struct 2009;Volume 20(5):575–85.
[21] Lu F, Lee HP, Lim SP. Modeling and analysis of micro piezoelectric power generators for micro-electromechanical-systems applications. Smart Mater Struct 2003;Volume 13(1):57–63.
[22] Múčka P. Simulated road profiles according to ISO 8608 in vibration analysis. J Test Eval 2017;46(1):20160265.
[23] Onoda J, Makihara K, Minesugi K. Energy-recycling semi-active method for vibration suppression with piezoelectric transducers. AIAA J 2003;Volume 41(4):711–19.
[24] Ottman GK, Hofmann HF, Bhatt AC, Lesieutre GA. Adaptive piezoelectric energy harvesting circuit for wireless remote power supply. IEEE Trans Power Electron 2002;Volume 17(5):669–76.
[25] Rajamani R. Vehicle dynamics and control, 2ed. New York: Springer; 2012.
[26] Roundy S. On the effectiveness of vibration-based energy harvesting. J Intell Mater Syst Struct 2005;Volume 16(10):809–23.
[27] Ruderman M, Kamiya Y, Iwasaki M. Extended lumped parameter electromechanical model of piezoelectric actuators. In: IEEE International Conference on Mechatronics (ICM 2015); 2015. p. 290–5.
[28] Ruderman M, Rachinskii D. Use of Prandtl-Ishlinskii hysteresis operators for coulomb friction modeling with presliding. J Phys: Conf Ser 2017;, Volume 811:012013.
[29] Rupitsch SJ. Piezoelectric sensors and actuators: fundamentals and applications. Springer; 2018.
[30] Savaresi SM, Poussot-Vassal C, Spelta C, Sename O, Dugard L. Semi-active suspension control design for vehicles. Elsevier; 2010.
[31] Shu Y, Lien I. Analysis of power output for piezoelectric energy harvesting systems. Smart Mater Struct 2006;Volume 15(6):1499.
[32] Shu YC, Lien IC. Efficiency of energy conversion for a piezoelectric power harvesting system. J Micromech Microeng 2006;Volume 16(11):2429–38.
[33] Sodano HA, Inman DJ, Park G. Comparison of piezoelectric energy harvesting devices for recharging batteries. J Intell Mater Syst Struct 2005;Volume 16(10):799–807.
[34] Tavares R, Molina JV, Al Sakka M, Dhaens M, Ruderman M. Modeling of an active torsion bar automotive suspension for ride comfort and energy analysis in standard road profiles. In: Preprints, Joint Conference 8th IFAC Symposium on Mechatronic Systems, and 11th IFAC Symposium on Nonlinear Control Systems; 2019. p. 584–9.
[35] Tavares R, Ruderman M. On energy harvesting using piezoelectric transducer with two-port model under force excitation. In: IEEE International Conference on Mechatronics (ICM); 2019. p. 414–19.
[36] Umeda M, Nakamura K, Ueha S. Analysis of the transformation of mechanical impact energy to electric energy using piezoelectric vibrator. Jpn J Appl Phys 1996;Volume 35(5S):3267.
[37] Wang Y, Inman DJ. A survey of control strategies for simultaneous vibration suppression and energy harvesting via piezoceramics. J Intell Mater Syst Struct 2012;Volume 23(18):2021–37.
[38] Yang Z, Erturk A, Zu J. On the efficiency of piezoelectric energy harvesters. Extreme Mech Lett 2017;Volume 15:26–37.
[39] Yang Z, Zu J. Comparison of PZN-PT, PMN-PT single crystals and PZT ceramic for vibration energy harvesting. Energy Convers Manage 2016;Volume 122:321–9.
[40] Zuo L, Tang X. Large-scale vibration energy harvesting. J Intell Mater Syst Struct 2013;Volume 24(11):1405–30.
[41] Zuo L, Zhang P-S. Energy harvesting, ride comfort, and road handling of regenerative vehicle suspensions. ASME J Vibr Acoust 2013;Volume 135(1):11002.

Rafael Tavares received the M.Sc. degree in Mechanical Engineering from the Faculty of Engineering of University of Porto (FEUP), Porto, Portugal, in 2014. During 2014–2018, he was Researcher at the Institute of Science and Innovation in Mechanical and Industrial Engineering (INEGI), Porto, Portugal. and in 2017 also Assistant Professor at FEUP, Porto, Portugal. In 2018 he enrolled the Ph.D. programme in Mechatronics at University of Agder (UiA), Grimstad, Norway. His current research interests are in model-based control, energy harvesting and smart materials.

Michael Ruderman received the B.Sc. degree in applied physics from the Polytechnical University of Kharkov, Kharkov, Ukraine, in 1997 and the Dipl.-Inf. degree in computer and electrical engineering and the Dr.-Ing. degree in electrical engineering from the Technical University (TU) Dortmund, Dortmund, Germany, in 2005 and 2012, respectively. During 2006–2013, he was Research Associate with the Institute of Control Theory and Systems Engineering, TU Dortmund. In 2013–2015, he was with Nagoya Institute of Technology, Nagoya, Japan, as specially appointed Assistant Professor. In 2015 he was specially appointed Associate Professor with the Department of Electrical Engineering, Nagaoka University of Technology, Nagaoka, Japan, before joining in the same year the University of Agder (UiA), Grimstad, Norway. He is member of the Faculty of Engineering and Science at UiA. His current research interests are in motion control, robotics, nonlinear systems with memory, and hybrid control systems. He is Associate Editor of IFAC Mechatronics journal and Technical Editor of IEEE/ASME Transactions on Mechatronics. He serves also as Chair of IEEE-IES Technical Committee on Motion Control.